Nanoscale

Dynamic Article Links

Cite this: *Nanoscale*, 2011, **3**, 4811

www.rsc.org/nanoscale

PAPER

Ultrathin conformal coating for complex magneto-photonic structures†

Oana Pascu,[a] José Manuel Caicedo,[a] Martín López-García,[b] Víctor Canalejas,[b] Álvaro Blanco,[b] Cefe López,[b] Jordi Arbiol,[ac] Josep Fontcuberta,[a] Anna Roig*[a] and Gervasi Herranz*[a]

Received 28th July 2011, Accepted 7th September 2011
DOI: 10.1039/c1nr10959f

We report on an extremely fast and versatile synthetic approach, based on microwave assisted sol–gel chemistry, that allows a conformal nanometric coating of intricate three-dimensional structures. Using this methodology, we have achieved a conformal coverage of large areas of three-dimensional opals with a superparamagnetic manganese ferrite layer, yielding magneto-photonic crystals with excellent quality. The use of a ternary oxide for the ultrathin coating demonstrates the potential of this methodology to realize three-dimensional structures with complex materials that may find applications beyond photonics, such as energy, sensing or catalysis.

1. Introduction

Keeping long-range structural order along the three dimensions (3D) is essential for the development of composite systems for different emerging areas, including metamaterials, magnonics, phononics and photonics.[1–4] Opals are one example of 3D ordering of sub-micronic spheres that have received much attention in recent years and which have strongly impacted the field of photonics. Fine tailoring of the photonic band gap and/or achieving new functionalities requires an appropriate coating of the 3D-opal structure by suitable materials while keeping the required high quality 3D structures. This is extremely challenging.[1,5,6] The most widespread methods to obtain 3D composite structures are atomic layer deposition, thermal chemical vapor deposition, electrodeposition[7] as well as deposition in aqueous solutions.[8–10] These methods, however, are limited by either the amount of available reagents and their relatively simple chemical formulations or the required long unpractical processing times.[8] We show here that microwave chemistry[11,12] is a very efficient method to achieve fast conformal ultrathin coating of opals with multivalent complex oxides, adding new functionalities to these photonic structures. Even though magnetophotonics is targeted here, applications to other areas, such as energy, as sensors or catalysis can be envisioned.

The addition of functional materials into photonic structures is an emergent field of research. In particular, the incorporation of magnetic materials in photonic crystals gives rise to intriguing new possibilities, including non-reciprocal optical effects[13] and large magneto-optical responses at the stop-band edge frequencies[14–16] with large potential in applications for optical communications. The promising results reported for one- (1D) and two-dimensional (2D) magneto-photonic crystals (MPCs)[17,18] have spurred research on 3D photonic crystals, in which the periodicity in the three dimensions should allow a better integration in devices with an enhanced functionality.[6,7,17,19] Nevertheless, efforts aimed at the achievement of 3D-MPCs are challenged by the difficulty of having the required high-quality long-range structure along the three directions in space and high magnetic content.[9,20–24]

Here, we report on a microwave assisted benzyl alcohol route that has allowed us the growth, in just a few minutes, of a stoichiometric and homogeneous conformal nanometric coating covering extensive areas—at least on the order of cm^2—of the 3D photonic crystals. The coating is formed by superparamagnetic $MnFe_2O_4$ nanoparticles and does not require any post-synthesis material processing (note that bulk $MnFe_2O_4$ is ferrimagnetic with a Curie temperature of ~560 K).[25] The resulting materials exhibit unambiguously enhanced magneto-photonic response at band edge frequencies and a magneto-optical response tunable by magnetic fields.

2. Experimental section

2.1 Microwave synthesis protocol

A non-aqueous benzyl alcohol route for ferrite nanoparticles, adapted from the one first reported by Niederberger,[12] was used. The microwave experiments were carried out using a CEM Discover reactor (Explorer 12-Hybrid) operating at a frequency of 2.45 GHz and a power of 200 W. Photonic crystals (direct SiO_2 and inverse Al_2O_3 opals) of about 5 mm × 5 mm in size grown on a glass slide substrate were vertically immersed in the reaction solution using a 10 ml closed pressurized vessel. The reaction media contained 0.3 mmol (sample I2) or 0.15 mmol (samples D1

[a]*Institut de Ciència de Materials de Barcelona (ICMAB-CSIC), Campus UAB, E08193 Bellaterra, Spain. E-mail: gherranz@icmab.es; roig@icmab.es*
[b]*Instituto de Ciencia de Materiales de Madrid (ICMM-CSIC), Calle Sor Juana Inés de la Cruz 3, Madrid, 28049, Spain*
[c]*Institució Catalana de Recerca i Estudis Avançats (ICREA), E08010 Barcelona, Spain*

† Electronic supplementary information (ESI) available. See DOI: 10.1039/c1nr10959f

and I1) of iron(III) acetylacetonate ($Fe(acac)_3$) and the stoichiometric quantity of manganese(II) acetate ($Mn(ac)_2$) with a total concentration of 0.3 M or 0.15 M in 1.5 ml of anhydrous benzyl alcohol. During a typical run, the power is automatically adjusted to heat the sample to 170 °C and the temperature is kept stable for 5 min. After the reaction takes place, the solution is automatically cooled to 60 °C by compressed nitrogen. Temperature and pressure are controlled by a volume independent infrared sensor.

2.2 Fabrication of direct and inverse opals

SiO_2 direct opals were fabricated by vertical deposition onto 1 cm width hydrophilic glass from a 1% (w/w) solution in ethanol at 55 °C and 60% relative humidity of the environment (in the oven). SiO_2 spheres of 260 nm diameter, synthesized by the Stöber method,[26] were used for the opal fabrication. Regarding the fabrication of Al_2O_3 inverse opals, direct opals of 320 nm (I1 and I2) and 276 nm (I1′) polystyrene spheres constituted the template for the inverse opal. The spheres were assembled by vertical deposition onto a hydrophilic glass substrate followed by infiltration of Al_2O_3 by atomic layer deposition (ALD, Savannah S100 Cambridge NanoTech Inc). Reactants for alumina growth, *i.e.*, trimethylaluminium (TMA) and water, were kept at room temperature. The sample, in the ALD vacuum chamber at 90 °C, was exposed to alternate TMA and water pulses (each with a duration of 10 ms). Each TMA–water cycle was followed by 5 s waiting time to ensure complete diffusion through the sample followed by 5 s chamber evacuation. The rate of alumina growth was about 0.18 nm per cycle as estimated by ellipsometry measurements. In our case, 80 cycles of ALD were used, forming an Al_2O_3 layer around 15 nm thickness. The inverse opals were produced by dissolving the polystyrene spheres with toluene.

2.3 Electron microscopy analysis

Transmission electron microscopy (TEM) was used for morphological and structural characterization. The high-resolution TEM images were obtained with a Jeol2010F field emission gun microscope working at 200 keV with a point to point resolution of 0.19 nm. The sample was prepared by scratching the coated opals and dispersing them in ethanol. Subsequently, after an ultrasound bath, a few drops of the solution were deposited on a TEM carbon grid, allowing the solvent to evaporate. During this TEM preparation, a significant portion of the oxide coating on the spheres was detached and, indeed, we observed in the TEM images a large amount of nanoparticles over the filaments of the carbon grids, probably deposited there after being separated from the opal surface during the preparation. Selected area diffraction patterns (SADP) were captured using a JEOL JEM-2011, operating at 200 kV.

SEM images were acquired using a Quanta FEI 200F microscope in low vacuum mode with a cone LOW kV P.L.A. type with 500 μm aperture. The working conditions were: an acceleration voltage of 10–20 kV, an electron beam spot of 2–2.5, a pressure of 50 Pa and a distance of 5–6 mm.

2.4 Magnetic circular dichroism

It was performed using a homemade experimental setup.[27,28] The sample on a holder was placed between the poles of an electromagnet. Light from a 150 W Xe arc lamp (ZolixTechnology) is dispersed by a monochromator (Zolix l-150), collimated, and then linearly polarized by the action of a Glan-Thompson prism, which is rotated 45° with respect to the modulator axis of a photo-elastic modulator (PEM). After the PEM, the light is transmitted through the sample (with a typical light beam diameter of about ~2 mm) and then goes toward a detector. The signal from this detector is brought to a lock-in amplifier synchronized to the frequency of the PEM retardation angle. It can be demonstrated that, in this setup configuration, one can measure the CD and MCD signals by inspection of the first harmonic of the detector signal.

3. Results and discussion

3.1 Microwave coating of opals

Microwave heating represents an attractive non-conventional energy source to perform chemical synthesis due to the high acceleration of the chemical reaction and the high yield obtained.[29,30] It is based on the ability of some compounds to absorb electromagnetic energy and to transform it into heat. While a domestic microwave has a multimode cavity producing a non-homogeneous heating of the cavity, the one for chemical synthesis is specially designed for a single mode, resulting in a uniform heating of the cavity. Compared to other conventional heating methods (heating plates and oil bath), the microwave radiation affects only the solvent and reactants, passing through the reaction vessel without heating it and avoiding any temperature gradients. While non-polar substances are not heated, microwaves produce a rapid, intense heating of polar substances permitting to have selective heating modes. In addition, microwaves induce molecular vibration and a subsequent temperature increase causing a greater movement of the molecules, a higher diffusivity and collision probability. Based on the heating selectivity and the increase of the molecular motion, complex nanostructured materials can be fabricated, as for instance, infiltration/doping of a structured/porous material with *in situ* synthesized secondary phase.[29,30] As a particular case, in this work we present *in situ* deposition of ferrite nanoparticles on preformed photonics crystals. The solvent used, benzyl alcohol, was employed for the first time as a microwave absorbing substance for iron oxide nanoparticle synthesis by Niederberger.[31] The preformed photonic crystals used by us were SiO_2 direct opals and Al_2O_3 inverse opals. In both cases, the hydroxyl terminated oxide surfaces of the Al_2O_3 and SiO_2 scaffolds are more susceptible to absorb microwave energy than the bulk of the material, activating in this way the opal surfaces and promoting the nucleation and the growth of the magnetic nanoparticles on these surfaces.

Before attempting the microwave-assisted growth of $MnFe_2O_4$ in photonic structures, the synthesis of self-standing ferrite nanoparticles has been optimized by adapting the non-aqueous sol–gel chemical reaction first reported by Niederberger *et al.*[9,32] Details of the synthesis as well as the material characterization are included in the Experimental section in the ESI†. By means of X-ray diffraction and magnetometry we identified the spinel structure of the nanoparticles with a mean diameter of ~5 nm (Fig. S1, ESI†). Pristine opals, direct (SiO_2) and inverse (Al_2O_3), with a period of 366 nm and 465 nm, respectively, and volumes of

~5 mm × 5 mm × ~0.5 μm were grown on glass slides by using known procedures.[26,33] Pristine direct opals have been labeled as D0 and inverse ones as I0. To load the opals with magnetic content, they were immersed in the reaction microwave vessel using iron(III) acetylacetonate and manganese(II) acetate as precursors. Two metal precursor concentrations were investigated while keeping the same microwave setup parameters: D1 and I1 refer to direct and inverse magnetic opals using a 0.15 M concentration and I2 when the concentration was 0.3 M.

Fig. 1 shows a series of scanning electronic microscopy (SEM) pictures of direct (Fig. 1a and b) and inverse (Fig. 1c and d) opals. The inspection of the images of the surface (Fig. 1a and c) and the cross-section (Fig. 1b and d) allows us to confirm the homogeneous and uniform coverage of the opal structures. The absence of coating in some particular places highlights the uniformity of the magnetic layer. For instance, the white circle at the right-hand side lower corner of Fig. 1a (direct opal) shows a small area where the coating is not complete; the coating is also absent in the contact points between two opal spheres (see Fig. 1b). Cross-sectional SEM pictures displayed in Fig. 1b–d show that the coating also reaches the deeper part of the crystals. Indeed SEM images obtained at different points over the cross-section—at the top, middle and bottom layers of the photonic crystals—show the continuous manganese ferrite layer visible until the bottom part of the direct opal (Fig. 2). A clue to the nature of this uniform conformal coverage is given by the observed superparamagnetic behavior that confirms that the coating is composed of magnetic nanoparticles. This conclusion is further confirmed by transmission electron microscopy (TEM) experiments. Fig. 1e displays a TEM image with an expanded view of the top of one of the silica particles forming the direct opal structure of Fig. 1a, where the ferrite nanoparticles can be observed. The analysis by means of high-resolution TEM confirms the expected cubic spinel structure. Indeed, selected area electron diffraction peaks (inset of Fig. 1e) can be indexed in the $MnFe_2O_4$ inverse spinel phase. A detailed HRTEM analysis was carried out on one of the nanoparticles oriented along the [001] zone axis (see a magnified detail in Fig. 1f), presenting the {220} and {400} family planes, further confirming the spinel structure. Electron energy loss spectroscopy (EELS) also corroborates the coating of the opal surfaces with $MnFe_2O_4$ nanoparticles (see Fig. S2 and S3 in the ESI†).

Previous works have also reported fairly high magnetic loads of nanoparticles embedded in direct opals, although the homogeneity of the infiltration was not fully addressed and long processing times (>24 h) were required.[8,9,23] In contrast, our 3D-MPCs have comparable volume fractions of the magnetic material—up to ~50% for direct opals, processed at a much faster speed—typically less than 30 min—and forming a quasi-ideal conforming coating. Additionally, no further thermal treatment of the composite material was required, since the magnetic material exhibited the desired inverse spinel crystalline phase structure ($MnFe_2O_4$). The degree of magnetic coverage

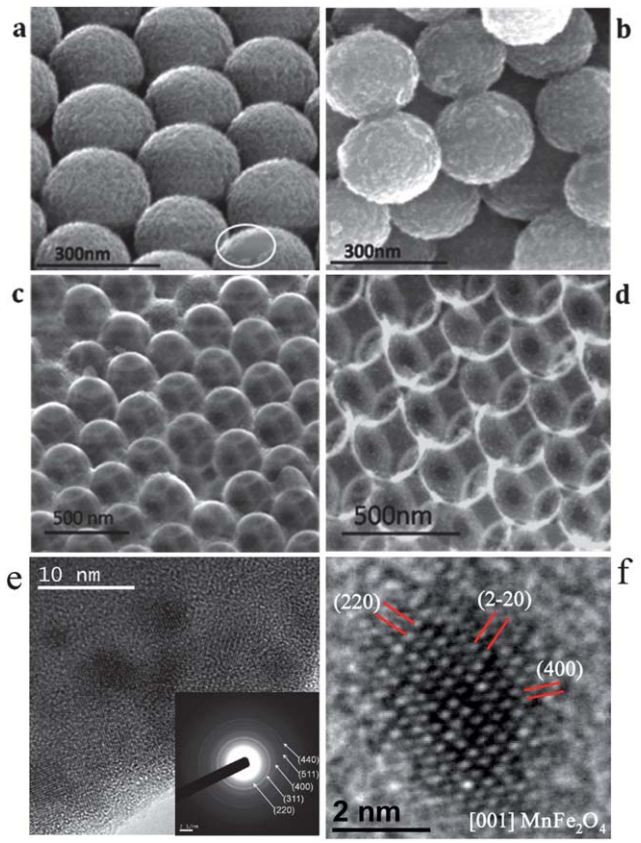

Fig. 1 Surface and cross-sectional SEM images have been obtained for direct (a and b) as well as inverse opals (c and d). Surface and cross-sectional SEM pictures assess the quality and uniformity of this coverage. (e) High-resolution TEM general image of one silica nanoparticle surface showing high density of crystalline ferrite nanoparticles. The inset corresponds to a selected area electron diffraction pattern obtained on the silica spheres. (f) Magnified detail of one of the inverse spinel nanoparticles.

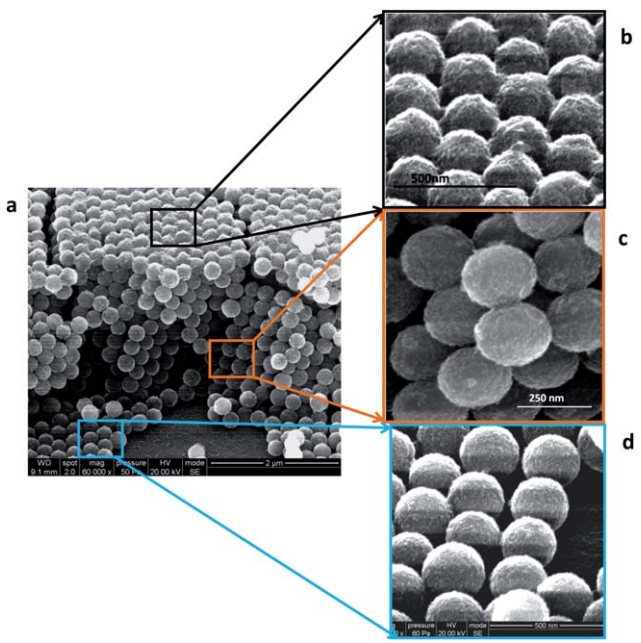

Fig. 2 (a) Overview SEM picture of direct opal (D1). Cross-sectional SEM pictures of the upper (b), middle (c) and bottom (d) layers of the photonic crystals. These images prove that the conformal $MnFe_2O_4$ magnetic coating is uniform across the depth of the photonic crystals.

could be achieved by controlling either the opal thickness or the duration of the reaction. First, the opal fabrication method by vertical colloidal self-assembly deposition yields opals with different thicknesses which in turn influences the microwave magnetic coating thickness. We have exploited this feature to find a magnetic loading with optimal functional properties. Fig. S4 in the ESI† presents SEM images of D1 material with different coverage degrees (a) as well as the optical (b) and magneto-optical measurements (c). On the other hand, Fig. S5 in the ESI† shows 3D-SiO_2 opals coated with γ-Fe_2O_3 nanoparticles where the influence of the reaction time on the degree of magnetic material coverage can be observed.

3.2 Optical and magneto-optical characterization

The excellent quality of the 3D-MPCs and the optimal coating with a magnetic layer revealed by the SEM and TEM images of Fig. 1 and 2 anticipates an optimal magneto-photonic response. To assess their functional properties, we have performed optical transmittance (OT) and magnetic circular dichroism (MCD) spectroscopy experiments in a range of wavelengths $\lambda = 400$–800 nm.[34] The spectra were taken at the same place (spot size $\approx$ 2 mm) to avoid the effects associated with any eventual spatial inhomogeneity.

OT experiments were undertaken to determine the stop-bands of the photonic crystals and to assess the influence of the magnetic coverage fraction on the optical properties. Although similar results were found in direct opals (see Fig. S4b in the ESI†), here we focus on the results obtained in the series of inverse opals (I0–I2). Fig. 3a shows the transmittance spectra of the pristine inverse opal (I0) as well as two magnetic opals with different concentrations (I1 and I2). We observe in Fig. 3a the presence of minima of the transmittance that signals the frequencies at which the stop-bands are centered. Thus the pristine I0 opal has the stop band centered on $\lambda_B \approx 517$ nm, whereas for the magnetic opals I1 and I2 the stop-bands are centered on $\lambda_B \approx 524$ nm and $\lambda_B \approx 534$ nm, respectively, revealing a red-shift due to the increasing magnetic coverage of the structures. Indeed, an inspection of the cross-sectional SEM images (Fig. 3c–e) demonstrates clearly how the shell thickness of the magnetic coating becomes larger with a major magnetic loading. We used these SEM cross-sectional images to determine the void ($\sim$300 nm) and the connecting window ($\sim$100 nm) diameters as well as the filling fractions $f_{air} = 0.87$ and $f_{Al2O3} = 0.13$ of air and alumina, respectively, in the inverse opal structures. These data were then used to quantify the magnetic filling fraction factors of the magnetic opals from the λ_B red-shift using the same method as we described previously,[35] yielding $f_{I1} = 0.0287$ (4.7% of the available pore volume) and $f_{I2} = 0.0704$ (11.5%) for I1 and I2, respectively. We show therefore that large magnetic load of the opals can be achieved and that the load can be controlled by the initial concentration of the precursors.

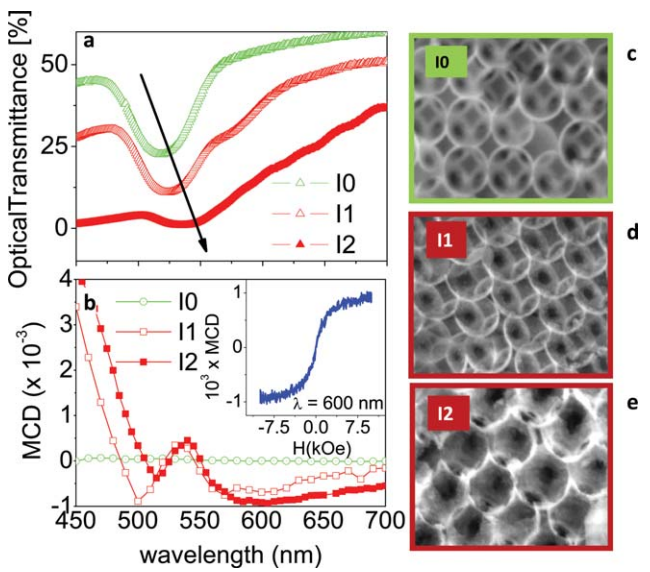

Fig. 3 Optical transmission (a) and magnetic circular dichroism (MCD) (b) data of the inverse opal structures I0–I2. I0 is the blank opal without magnetic content, whereas I1 and I2 are opals with different concentrations of magnetic loading (see the text). The different degrees of coating (see SEM pictures on panels (c–e) on the cross-section of the infiltrated inverse opals) and the resulting different amounts of magnetic material infiltration can be monitored by optical measurements through the progressive red-shift of the optical stop band (a). The inset of (b) shows a MCD hysteresis loop measured at $\lambda = 600$ nm. The maximum value of these loops (at $H = 1$ Tesla) for each wavelength was used to plot the MCD spectra shown in (b).

To obtain the intrinsic magneto-optic response of opals—free of the optical activity inherent in their structure (ref. 36)—we recorded the whole series of full MCD hysteresis loops for wavelengths in the visible range and obtained the MCD spectral response from the amplitude of the loops. Following this approach, we have observed a null MCD spectral signal on the blank inverse opal I0, as expected from the absence of magnetic content in this sample (Fig. 3b). Instead, the samples loaded with the magnetic content (I1 and I2) exhibit MCD loops (inset of Fig. 3b). We have measured these loops for a range of wavelengths and plot the MCD spectral response from their amplitude signal (open circles, Fig. 3b). We observe that an intricate structure appears in the MCD spectra around the stop-band regions (Fig. 3a), indicating that a magneto-photonic response develops due to the interplay of the photonic and magneto-optical properties.

To better understand the relationship between the photonic band structure and magneto-optics, we compare the magneto-photonic response of direct and inverse opals. Fig. 4 shows the MCD spectra (right axis) of a direct SiO_2 opal of 366 nm periodicity and 10.4% filling factor (D1, Fig. 4a) and two Al_2O_3 inverse opals of different periodicity, 465 nm with 4.7% filling factor (I1, Fig. 4b) and 276 nm with 0.6% (labeled as I′1, it was processed in the same conditions as I1, Fig. 4c). Fig. 4 also includes the OT spectra (left axis) of each of these crystals as well as the MCD spectrum of $MnFe_2O_4$ nanoparticles distributed randomly on a glass substrate. The latter gives the magneto-optical response of $MnFe_2O_4$ nanoparticles in the absence of any photonic effect. A common feature observed for all the magnetic opals is that the MCD response is deeply modified with respect to that of the randomly distributed nanoparticles, indicating that the photonic band structure of the crystals radically influences the magneto-optical properties of the manganese ferrite nanoparticles. Interestingly, we observe that the magneto-optical signal is enhanced at the stop-band edges (even for very low

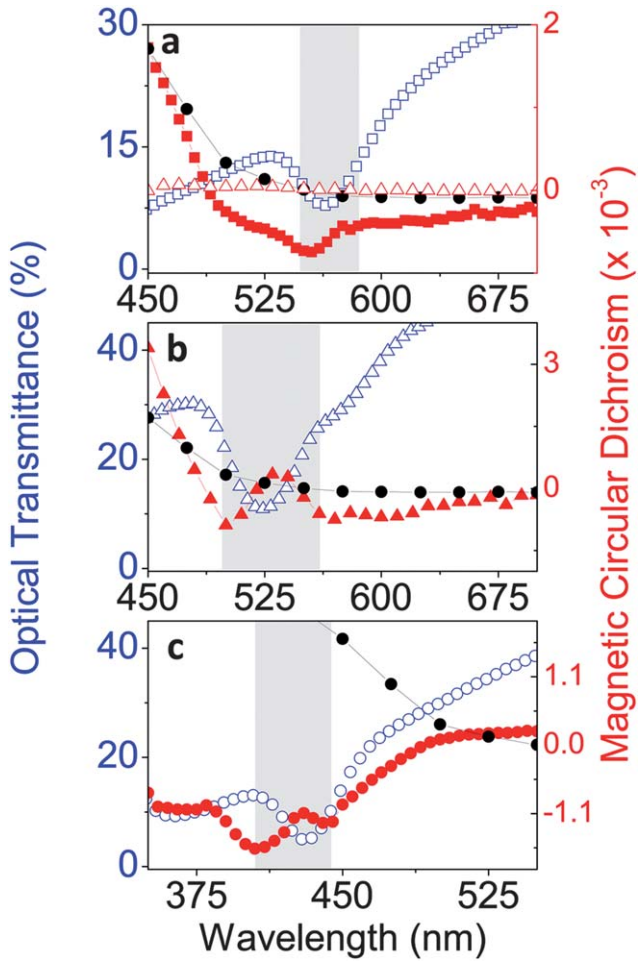

Fig. 4 MCD and OT spectra obtained in a direct opal D1 (a) and two different inverse opals I1 (b) and I′1 (c) with different periodicity. Panel (a) also includes the MCD spectra of a blank opal without magnetic loading (empty red triangles). All of them show anomalous features at the stop band edges (the stop band area is shaded), although the major effects are seen in inverse opals. We show in these figures the spectra of randomly distributed $MnFe_2O_4$ nanoparticles (black solid circles) that are the reference of the magneto-optic spectral response free of any magneto-photonic effect.

filling factor), as observed in the shaded areas of Fig. 4. This signal enhancement is particularly large in the inverse opals, and more specifically for the opal I′1 where two prominent shoulders are well visible, indicating that in the vicinity of the band-edge frequencies the influence of the photonic structure on the magneto-optics is very intense. An important observation is that the optical transmittance of the inverse opals is larger than that of the direct opal. A huge magneto-photonic effect in combination with a good optical transmittance makes these complex materials very appealing for applications in optical communications.

Finally, note that all the materials comprising the photonic structures here described are dielectric and, thus, such structures do not support the propagation of surface plasmon polaritons. Thus, the enhanced magneto-optical response is the result of the strong interaction of light with the structure close to the photonic band frequencies (where the Bragg reflection condition is fulfilled), rather than coupling to plasmons, as recently reported for other systems combining magnetic materials and noble metals.[37] The use of a dielectric photonic crystal to enhance the magneto-optic signal has the advantage of minimizing the optical losses that otherwise would be detrimental for many applications in optical communications.

4. Conclusions and outlook

We have presented an extremely fast and versatile microwave assisted sol–gel route to achieve the conformal coverage of large areas of three-dimensional opals with a superparamagnetic manganese ferrite layer. The use of a ternary oxide for ultrathin coating demonstrates the potential of this methodology to realize three-dimensional structures with complex materials. The resulting materials exhibit unambiguously enhanced magneto-photonic response at band edge frequencies and a magneto-optic response tunable by magnetic fields. The strategy presented here will contribute to the rapidly expanding field of advanced techniques for the fabrication of three-dimensional complex systems needed in different fields such as in photonics, phononics, metamaterials or data storage. The approach could also be relevant for some applications in materials for energy, as for instance in sensors, or in catalysis where a full coverage with functional materials on intricate topologies is crucial to boost the device performance.

Acknowledgements

Authors warmly acknowledge discussions on microwave synthesis with Susagna Ricart (ICMAB-CSIC) and on optical and magneto-optical properties with Antonio García Martín and Gaspar Armelles (CNM-CSIC). We also acknowledge partial financial support from the CSIC CRIMAFOT (PIF 08-016), the Spanish Government (CONSOLIDER Nanoselect-CSD2007-00041 and NanoLight.es-CSD20070046, MAT2008-06761-C03, MAT2011-29269-C03-01, MAT2009-08024, MAT2009-06885-E, MAT2009-07841 and FPI grant of J.M.C.), the Generalitat de Catalunya (2009SGR-376, 2009SGR-203 and FI grant of O.P.), the Comunidad de Madrid S-0505/ESP-0200 and the EC FP7 NoE Nanophotonics4Energy-248855.

References

1 M. Farsari and B. N. Chichkov, *Nat. Photonics*, 2009, **3**, 450–452.
2 V. V. Kruglyak, S. O. Demokritov and D. Grundler, *J. Phys. D: Appl. Phys.*, 2010, **43**, 264001.
3 E. Yablonovitch, *Nature*, 2009, **461**, 744–745.
4 J. B. Pendry, D. Schurig and D. R. Smith, *Science*, 2006, **312**, 1780–1782.
5 A. Blanco, E. Chomski, S. Grabtchak, M. Ibisate, S. John, S. W. Leonard, C. Lopez, F. Meseguer, H. Miguez, J. P. Mondia, G. A. Ozin, O. Toader and H. M. van Driel, *Nature*, 2000, **405**, 437–440.
6 S. Noda, K. Tomoda, N. Yamamoto and A. Chutinan, *Science*, 2000, **289**, 604–606.
7 X. Yu, Y.-J. Lee, R. Furstenberg, J. O. White and P. V. Braun, *Adv. Mater.*, 2007, **19**, 1689–1692.
8 S. A. Grudinkin, S. F. Kaplan, N. F. Kartenko, D. A. Kurdyukov and V. G. Golubev, *J. Phys. Chem. C*, 2008, **112**, 17855–17961.
9 V. V. Pavlov, P. A. Usachev, R. V. Pisarev, D. A. Kurdyukov, S. F. Kaplan, A. V. Kimel, A. Kirilyuk and Th. Rasing, *Appl. Phys. Lett.*, 2008, **93**, 072502–072503.

10 A. V. Baryshev, T. Kodama, K. Nishimura, H. Uchida and M. Inoue, *J. Appl. Phys.*, 2004, **95**, 7336–7338.
11 I. Bilecka and M. Niederberger, *Nanoscale*, 2010, **2**, 1358–1367.
12 I. Bilecka, M. Kubli, E. Amstad and M. Niederberger, *J. Sol-Gel Sci. Technol.*, 2011, **57**, 313–322.
13 Z. Wang, Y. Chong, J. D. Joannopoulos and M. Soljačić, *Nature*, 2009, **461**, 772–775.
14 K. Takahashi, F. Kawanishi, S. Mito, H. Takagi, K. H. Shin, J. Kim, P. B. Lim, H. Uchida and M. Inoue, *J. Appl. Phys.*, 2008, **103**, 07B331.
15 J. V. Boriskina, S. G. Erokhin, A. B. Granovsky, A. P. Vinogradov and M. Inoue, *Phys. Solid State*, 2006, **48**, 717–721.
16 A. A. Fedyanin, O. A. Aktsipetrov, D. Kobayashi, K. Nishimura, H. Uchida and M. Inoue, *J. Magn. Magn. Mater.*, 2004, **282**, 256–259.
17 M. Inoue, R. Fujikawa, A. Baryshev, A. Khanikaev, P. B. Lim, H. Uchida, O. Aktsipetrov, A. Fedyanin, T. Murzina and A. Granovsky, *J. Phys. D: Appl. Phys.*, 2006, **39**, R151–R161.
18 A. K. Zvezdin and V. I. Belotelov, *Eur. Phys. J. B*, 2004, **37**, 479–487.
19 A. Mekis, J. C. Chen, I. Kurland, S. Fan, P. Villeneuve and J. D. Joannopoulos, *Phys. Rev. Lett.*, 1996, **77**, 3787–3790.
20 N. Liu, H. Guo, L. Fu, S. Kaiser, H. Schweizer and H. Giessen, *Nat. Mater.*, 2008, **7**, 31–37.
21 M. Fang, T. T. Volotinen, S. K. Kulkarni, L. Belova and K. V. Rao, *J. Appl. Phys.*, 2010, **108**, 103501–103506.
22 I. Šimkiene, A. Reza, A. Kindurys, V. Bukauskas, J. Babonas, R. Szymczak, P. Aleshkevych, M. Franckevicius and R. Vaišnoras, *Lith. J. Phys.*, 2010, **50**, 7–15.
23 V. V. Pavlov, P. A. Usachev, R. V. Pisarev, D. A. Kurdyukov, S. F. Kaplan, A. V. Kimel, A. Kirilyuk and Th. Rasing, *J. Magn. Magn. Mater.*, 2009, **321**, 840–842.
24 J. M. Caicedo, E. Taboada, D. Hrabovsky, M. Lopez-Garcıa, G. Herranz, A. Roig, A. Blanco, C. Lopez and J. Fontcuberta, *J. Magn. Magn. Mater.*, 2010, **322**, 1494–1496.
25 Z. X. Tang, C. M. Sorensen, K. J. Klabunde and G. C. Hadjipanayis, *Phys. Rev. Lett.*, 1991, **67**, 3602.
26 J. F. Galisteo-López, M. Ibisate, R. Sapienza, L. S. Froufe-Perez, A. Blanco and C. López, *Adv. Mater.*, 2011, **23**, 30–69.
27 J. M. Caicedo, M. C. Dekker, K. Dörr, J. Fontcuberta and G. Herranz, *Phys. Rev. B: Condens. Matter Mater. Phys.*, 2010, **82**, 140410–140414.
28 J. M. Caicedo, S. K. Arora, R. Ramos, I. V. Shvets, J. Fontcuberta and G. Herranz, *New J. Phys.*, 2010, **12**, 103023–103028.
29 A. de la Hoz, A. Diaz-Ortiz and A. Moreno, *Chem. Soc. Rev.*, 2005, **34**, 164–178.
30 P. Lidstrom, J. Tierney, B. Wathey and J. Westman, *Tetrahedron*, 2001, **57**, 9225–9283.
31 N. Pinna, S. Grancharov, P. Beato, P. Bonville, M. Antonietti and M. Niederberger, *Chem. Mater.*, 2005, **17**, 3044–3049.
32 I. Bilecka and M. Niederberger, *Chem. Commun.*, 2008, 886–888.
33 P. Jiang, J. F. Bertone, K. S. Hwang and V. L. Colvin, *Chem. Mater.*, 1999, **11**, 2132–2140.
34 O. Pascu, J. M. Caicedo, J. Fontcuberta, G. Herranz and A. Roig, *Langmuir*, 2010, **26**, 12548–12552.
35 J. M. Caicedo, O. Pascu, M. López-García, V. Canalejas, A. Blanco, C. López, J. Fontcuberta, A. Roig and G. Herranz, *ACS Nano*, 2011, **5**, 2957–2963.
36 A. Blanco, C. López, R. Mayoral, H. Míguez, F. Meseguer and J. Herrero, *Appl. Phys. Lett.*, 1998, **73**, 1781–1783.
37 V. I. Belotelov, I. A. Akimov, M. Pohl, V. A. Kotov, S. Kasture, A. S. Vengurlekar, A. V. Gopal, D. R. Yakovlev, A. K. Zvezdin and M. Bayer, *Nat. Nanotechnol.*, 2011, **6**, 370–376.

